

Dynamic Simulation Analysis of the Working Device of a ZL50 Loader

Guiju Zhang^{1,2} and Caiyuan Xiao^{1,2,*}

¹Key Laboratory of Hunan Province for Efficient Power System and Intelligent Manufacturing, Shaoyang, 422000, China

²College of Mechanical and Energy Engineering, Shaoyang University, Shaoyang, 422000, China

*Corresponding Author: Caiyuan Xiao. Email: xiaocaiyuan1999@sina.com

Received: 19 December 2019; Accepted: 23 April 2020

Abstract: In this study, assuming a certain type of wheel loader as the main objective of the research, the performances of the working device of the loader are investigated on the basis of an in-house code. After creating a three-dimensional model of the working device using Solidworks, this model has been imported into the dynamic simulation software ADAMS, and the simulation problem has been completed by adding the relevant constraints and loadings. The load stress curve relating to the main connecting point of the working device has been obtained in the frame work of this approach and it has been shown that the movement characteristics are compatible with (i.e., they match) the actual working conditions. The present study may be regarded as a theoretical basis for the design and improvement of the working device of a vast category of wheel loaders.

Keywords: ADAMS; working device; solidworks; wheel loader; dynamic simulation

1 Introduction

Wheel loader is the main construction machinery in the field of mechanical engineering. The working device is one of the important components of the wheel loader and the construction tool for the direct work of the wheel loader. When in use, the movement and force are complex, and loader's stability and reliability directly affect the working quality and efficiency [1–4]. Compared with other engineering machinery products, although more extensive research has been carried out in the field of wheel loader design, the design of its working device is still based on imitation design and its working efficiency is low. It is of great theoretical significance and engineering value to systematically study the dynamic characteristics of the working device and the key parts of the wheel loader. In this paper, it takes the resistance characteristics of the working device of the wheel loader as the function objective and the position of the connection point of the working device as a variable, the change of the constrained reaction force at the key connection point of the working device is obtained by the simulation calculation of the ADAMS software. The calculation results provide the basis for the design and improvement of the working device of various types of wheel loaders [5–7]. The research object of this paper is selected some certain type of ZL50 wheel loader.



This work is licensed under a Creative Commons Attribution 4.0 International License, which permits unrestricted use, distribution, and reproduction in any medium, provided the original work is properly cited.

2 Working Device Modeling

As shown in Fig. 1, the working device of loader is composed of bucket, boom, connecting rod and rocker arm etc. [8]. The working range of the working device is mainly determined by the stroke of the hydraulic cylinder. The basic parameters of the working device are shown in Tab. 1 [9,10]. According to the physical prototype size measured by the actual wheel loader, the 3D modeling is established by using Solidworks software. And then it is introduced into the multi-body dynamics software ADAMS to carry out dynamics simulation after applying material properties and constraints on the 3D modeling. The size of loads' bucket, boom, connecting rod, rocker arm, oil cylinder of rocker arm are related standard size of ZL50 Loader in [11–13]. The purpose of the research is to make a more detailed simulation analysis of several typical working conditions for the loader, so as to get the simulation results more covering, which can support the argument.

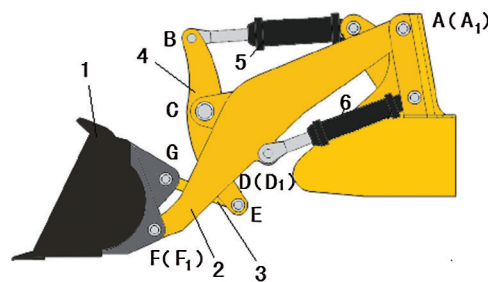


Figure 1: Working device assembly drawing of wheel loader. 1—bucket; 2—boom; 3—connecting rod; 4—rocker arm; 5—oil cylinder of rocker arm; 6—arm lift cylinder

Table 1: Basic parameters of working device

Item	Value	Item	Value
Rated capacity (kg)	5000	Discharge height (mm)	2970
Working quality (kg)	16800	Maximum rise force (kN)	167
Power rating (kw)	162	Overall weight (t)	17.5
Bucket capacity (m ³)	3	Maximum tractive force (kN)	145

3 Load Calculation of Working Device

Loader operation flow can be divided into six stages: inserting, bucketing, transporting, lifting, unloading and releasing. The main resistance F_1 in the process of operation is bucket insert material pile when the insert resistance. The instantaneous shovel resistance F_2 produced during shovel loading and the G composition of material gravity in the lifting process of the boom [14].

The real working temperature for the typical operating conditions is normal atmospheric temperature.

The insert resistance F_1 is the reaction force of the bucket to the bucket in the process of inserting the bucket. The resistance of the cutting edge and the front cutting edge of the two sides of the bucket, the friction resistance between the inside surface of the side wall and the bottom of the bucket and the material are respectively used. Friction resistance on the outer surface of the bucket when in contact with the material. The insert resistance F_1 usually related to the type of material, height of the pile, depth of the bucket inserted into the pile, structure of the bucket, etc. [15]. It can be calculated by empirical formula [16].

$$F_1 = 9.8K_1K_2K_3K_4BL^{1.25} \quad (1)$$

where, F_1 is the resistance when bucket is inserted with the unit is Newton; K_1 is the material loose coefficient valued from 0.1 to 1.3; K_2 is the material property coefficient with valued from 0.45 to 1.3; K_3 is the influence coefficient of pile height with valued from 0.55 to 1.15; K_4 is the bucket shape coefficient with valued as 1.5; B is the bucket width with valued as 300 cm; L is the bucket insertion depth with valued as 40 cm.

The shovel resistance F_2 is the reaction force of the pile to the bucket related to the material type. It can be calculated from the following formula

$$F_2 = 2.2KBL \quad (2)$$

where, K is the shear stress of the material at the beginning of the lifting with value as 35,000 Pa; B is the bucket width with value as 300 cm; L is the bucket insertion depth with value as 40 cm.

By substituting the above parameters in the formulas (1) and (2), it can be obtained that:

$$F_1 = 101238 \text{ N}, F_2 = 92400 \text{ N}, G = 149573 \text{ N} \quad (3)$$

4 Function Control

4.1 ADAMS Basic Dynamics Algorithm for Multibody Systems

4.1.1 Establishing the Motion Equations

In the research field of multibody dynamics systems, inertial systems are often used as reference systems. Through body pair a homogeneous rectangular coordinate system can clearly define the position of the spatial rigid body B_i . That is to say, using the unit vector Coordinate system alignment: $\vec{e}_{ix}, \vec{e}_{iy}, \vec{e}_{iz}$ indicates the rigid body position. Defining the origin of a rigid body B_i centroid based on a reference system i of point coordinates $\vec{e}_{ix}, \vec{e}_{iy}, \vec{e}_{iz}$ and position vecto $\vec{r}_i(3 \times 3)$ and rotation matrix $A_i(3 \times 3)$.

The displacement vector of the free body is defined according to the centred F through three instructed coordinates and is displayed as a column matrix in system I.

$$\vec{r}_i = r_{ix/I} \vec{e}_{ix} + r_{iy/I} \vec{e}_{iy} + r_{iz/I} \vec{e}_{iz} \quad (4)$$

$$\vec{r}_{ix} = \begin{bmatrix} r_{ix/I} \\ r_{iy/I} \\ r_{iz/I} \end{bmatrix} \quad (5)$$

A rotation matrix is a function of three amplitudes that can be rotated by Euler, Kardanic angles and three units matrix (rotating around coordinate axis) to be defined.

The rotation matrix can be written as

$$A_{ii} = A_{IK}(\alpha) A_{Kj}(\beta) A_{Jl}(\gamma) = \begin{bmatrix} c\beta c\gamma & -c\beta s\gamma & s\beta \\ c\alpha c\gamma + s\alpha s\beta c\gamma & c\alpha s\gamma + s\alpha s\beta s\gamma & -s\alpha c\beta \\ s\alpha s\gamma - c\alpha s\beta c\gamma & s\alpha c\gamma + c\alpha s\beta s\gamma & c\alpha c\beta \end{bmatrix} \quad (6)$$

where, abbreviations $\sin\alpha = sa$, $\cos\alpha = ca$. B_i displacement of a single free body can be determined according to six degrees of freedom. A vector representing six generalized coordinates through displacement $[6 \times 1]$.

$$Z = [r_{xi} \quad r_{yi} \quad r_{zi} \quad \alpha_i \quad \beta_i \quad \gamma_i] \quad (7)$$

Displacement vector and rotation matrix can be respectively expressed as functions of displacement vector Z .

$$A_{li} = A_{li}(Z), r_{i/I} = r_{i/I}(Z) \quad (8)$$

The velocity of centroid B_i can be calculated as a reference system I

$$V_{i/I} = \frac{dr_{i/I}}{dt} = \frac{\partial r_{i/I}}{\partial z} Z \quad (9)$$

The equation of centroid displacement can be described by a Jacobi matrix of $[6 \times 3]$

$$V_{i/I} = J_{Ci/I} Z = \begin{bmatrix} 1 & 0 & 0 & 0 & 0 & 0 \\ 0 & 1 & 0 & 0 & 0 & 0 \\ 0 & 0 & 1 & 0 & 0 & 0 \end{bmatrix} \begin{bmatrix} \dot{r}_{xi} \\ \dot{r}_{yi} \\ \dot{r}_{zi} \\ \dot{\alpha}_i \\ \dot{\beta}_i \\ \dot{r}_i \end{bmatrix} \quad (10)$$

or simplification without reference system I

$$V_i = J_{Ci} Z \quad (11)$$

By the same token, angular velocity can be calculated by Jacobi rotation matrix

$$\omega_i = J_{\omega i} Z \quad (12)$$

$$J_{\omega i} = \begin{bmatrix} 0 & 0 & 0 & 1 & 0 & s\beta \\ 0 & 0 & 0 & 0 & c\alpha & -s\alpha c\beta \\ 0 & 0 & 0 & 0 & s\alpha & c\alpha c\beta \end{bmatrix} \quad (13)$$

Angular velocity and dynamic freedom can be defined by motion constraints between bodies. A processing system contains q the total number of degrees of freedom of independent generalized coordinates can be expressed as $f = 6p - q$ for p rigid body system with constraints.

For the determination of multi-body equations of motion, the second Lagrange equation is generally expressed by the following two methods (Second Kind Lagrange Equations) and establishment of the Newton-Euler equation of motion (Newton-Euler Equations).

4.1.2 Kinematics Analysis

The kinematic analysis is research position, velocity, acceleration and constraint reaction of the system with zero degrees of freedom. Solving System Constraint Equations are as follows:

$$\phi(q, t) = 0 \quad (14)$$

q_0 is known already.

Any time position can be determined by Newton-Raphson iteration of constraint equation

$$\frac{\partial \phi}{\partial q} \Big|_{\Delta q_j} = -\phi(q_i, t_n) \quad (15)$$

where, $\Delta q_j = q_{j+1} - q_j$, j Represents a fifth iteration.

The determination of time velocity and acceleration can be obtained from the first and second order time derivatives of the constraint equation:

$$\frac{\partial \phi}{\partial q} q = -\phi \left(\frac{\partial \phi}{\partial t} \right) \quad (16)$$

$$\frac{\partial \phi}{\partial q} q = - \left\{ \frac{\partial^2 \phi}{\partial t^2} + \sum_{k=1}^n \sum_{l=1}^n \frac{\partial^2 \phi}{\partial q_k \partial q_l} q_k q_l + \frac{\partial}{\partial q} \left(\frac{\partial \phi}{\partial t} \right) q \right\} \quad (17)$$

The constraint reaction force at t_n can be determined by Lagrangian equation with multiplier

$$\left(\frac{\partial \phi}{\partial q} \right)^T \lambda = \left\{ \frac{d}{dt} \left(\frac{\partial T}{\partial q} \right) + \left(\frac{\partial T}{\partial q} \right)^T + Q \right\} \quad (18)$$

4.2 Design of Experiments in ADAMS

Experimental design (Design of Experiments, DOE) considering simultaneous changes in multiple design variables the influence of each design variable on the performance of the prototype. The experimental design includes establishment of design matrix and its results statistical analysis, etc. Initially, the designed experimental design (DOE) was used for physical experiments, but for virtual the effect of the test is also very good. Conventional DOE is time-consuming and laborious. Use ADAMS DOE can increase Add credibility to the results, and at the speed of the results compared to the trial-and-error test or one test at a time. The experiment of factor is faster, at the same time, it can help users better understand and optimize the mechanical system performance.

For simple design problems, you can mix empirical knowledge, trial-and-error methods, or powerful methods used to explore and optimize the performance of mechanical systems. But these methods can not be derived when the design scheme increases quick, systematic formulaic answers. It indicates that the factors will influence each other, and it can be obtained to test many different factors at the same time through many simulations to a large amount of output data for user evaluation. For less time-consuming work, ADAMS/Insight provide a Customize planning and analysis tools to conduct a series of trials and ADAMS/Insight help identify relevant data are analyzed, and the whole test design process is completed automatically.

Overall, the DOE in the ADAMS is a set of steps and systems for the organization and analysis of test results. The purpose of the test is to measure the performance of the virtual prototype model, the output of the manufacturing process, or the Improvement of product quality.

4.3 Driving Function Control

In the excavating operation of loader, first the bucket is inserted into the material, then the bucket is shoveled up, the insertion resistance and the shovel resistance reach the maximum in turn. The gravity of each component and material, by defining the magnitude and direction of the gravitational acceleration [17]. In this paper, the author uses an in-house code. That is, the program language code of ADAMS, and the program is completely completed on the platform of ADAMS simulation software.

The hydraulic pressure is the source of the motion Furthermore, the time step are also described in the simulation work. The hydraulic cylinder motion is mainly driven by the application of STEP function. The specific settings are as follows:

(a) Driving equation of bucket cylinder

step(time, 0, 0, 2.5, 0) + step(time, 2.5, 0, 5, -245) + step(time, 5, 0, 6.5, 0) + step(time, 6.5, 0, 10, 0) + step(time, 10, 0, 12.5, 285) + step(time, 12.5, 0, 13, 0) + step(time, 13, 0, 15, -40)

(b) Driving equation of boom cylinder

$\text{step}(\text{time}, 0, 0, 2.5, 0) + \text{step}(\text{time}, 2.5, 0, 5, 0) + \text{step}(\text{time}, 5, 0, 6, -40) + \text{step}(\text{time}, 6, 0, 6.5, 0) + \text{step}(\text{time}, 6.5, 0, 10, -720) + \text{step}(\text{time}, 10, 0, 12.5, 0) + \text{step}(\text{time}, 12.5, 0, 15, 760)$

4.4 Load Function Control

Functions F_1 of and F_2 are expressed in the ADAMS are as follows:

The insert resistance F_1 :

$\text{step}(\text{time}, 0, 0, 2.2, 101238) + \text{step}(\text{time}, 2.2, 0, 2.5, -101238) + \text{step}(\text{time}, 2.5, 0, 15, 0)$

The shovel resistance F_1 :

$\text{step}(\text{time}, 0, 0, 2.5, 0) + \text{step}(\text{time}, 2.5, 0, 2.7, 92400) + \text{step}(\text{time}, 2.7, 0, 5, -92400) + \text{step}(\text{time}, 5, 0, 15, 0)$

The material gravity G:

$\text{step}(\text{time}, 0, 0, 2.7, 0) + \text{step}(\text{time}, 2.7, 0, 5, 49573) + \text{step}(\text{time}, 5, 0, 10, 0) + \text{step}(\text{time}, 10, 0, 12.3, -49000) + \text{step}(\text{time}, 12.3, 0, 15, 0)$

Fig. 2 shows the step function curve of bucket cylinder and boom cylinder. And the function curves of insert resistance, shovel resistance and material gravity G are shown in Fig. 3.

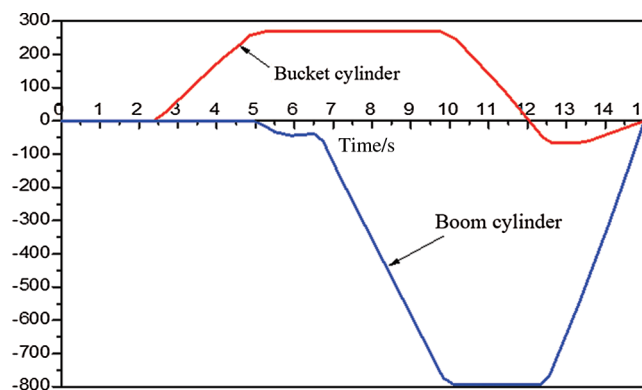


Figure 2: Step function curve of bucket cylinder and boom cylinder

5 Simulation Analysis

5.1 Force Simulation Analysis of Hydraulic Cylinder

In the process of simulation, the simulation time is 15 s and the number of simulation steps is 200. The displacement and load change of each important component and its hinge point are calculated by ADAMS.

Fig. 4 shows the force simulation curves of the boom cylinder and the bucket cylinder during the construction process. In Fig. 4, from 0 to 2.5 s the working device is in the horizontal insertion stage and the bucket bears the insert resistance. At this stage, the cylinder of the arm and bucket fluctuate and the force of the cylinder is a little larger, synchronously reaches the maximum value at 2.2 s afterwards the traction force of the engine decreases. At 2.5–5 s, the force of bucket cylinder and arm cylinder increased with the increase of shovel resistance, and at 4.5 s or so. When the cylinder pressure reaches the maximum value 4.5 s, the cylinder pressure decreases gradually with the decrease of resistance. The time 5–12 s is the lifting stage, the bucket oil cylinder is in the locked state and increases with the lift height. The length of boom cylinder increased together with the pressure of cylinder increased slightly, finally the force of bucket oil cylinder decreased. The time 10.5–12.5 s was the unloading stage where the cylinder of arm was in the state of locking. With the decrease of load, the force of the boom cylinder

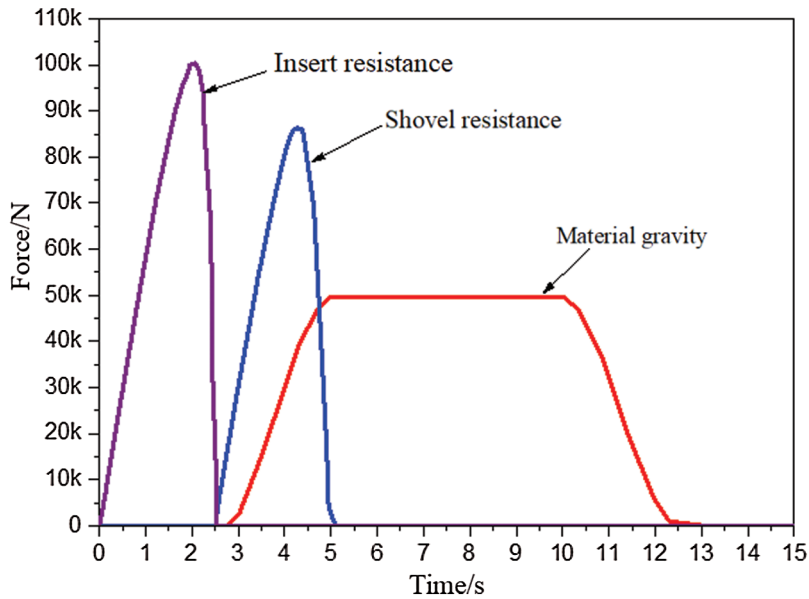


Figure 3: Load curves of working device

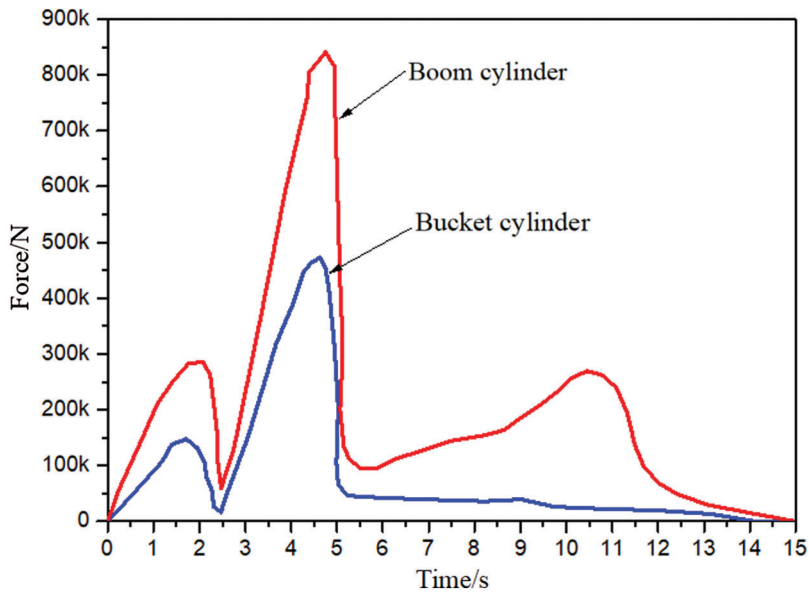


Figure 4: The force curves of boom cylinder and the bucket cylinder

decreases gradually. The time 12.5–15 s, the pressure fluctuation of each hydraulic cylinder is small, and the force of the boom cylinder is slightly larger than that of the bucket cylinder.

5.2 Simulation Analysis of the Force on the Hinge Points of the Loader’s Working Device

Fig. 5 shows the force simulation curves of each hinge point for the working device. In the horizontal insertion stage, the load on each hinge point increases with the increase of bucket insertion depth, and reaches the maximum local force at 2.5 s where the curve appeared first peak. After the insert action was completed, the bucket entered the flip operation where the second peak value appeared as the bucket flipped. That is, the curve reached the maximum value of the simulation at 2.8 s of the whole force. At this time, the stress of each

hinge point reaches the maximum value and the maximum stress value of 930 kN appears at the hinge of the arm and the front support, and then the stress value of each hinge point drops rapidly. At 5 s, the working device enters the lifting stage. As source of lift power is the hydraulic pressure of the moving wall oil cylinder, the simulation curve of hinge point at the two ends of the moving arm oil cylinder appears a smaller wave peak. At 10.5 s, it begins to unload material and stress values of each hinge point accordingly decreasing with the end of the unloading stage. From the analysis results of Fig. 5, the concentrated stress value at the joint between arm and other members is higher, which is easy to be damaged in the process of operation. The strength and stiffness factors should be taken into account in the structural design. High strength alloy steel materials are used in the joint shaft. The surface of the connection shaft is polished and polished to improve its fatigue strength and prolong its service life.

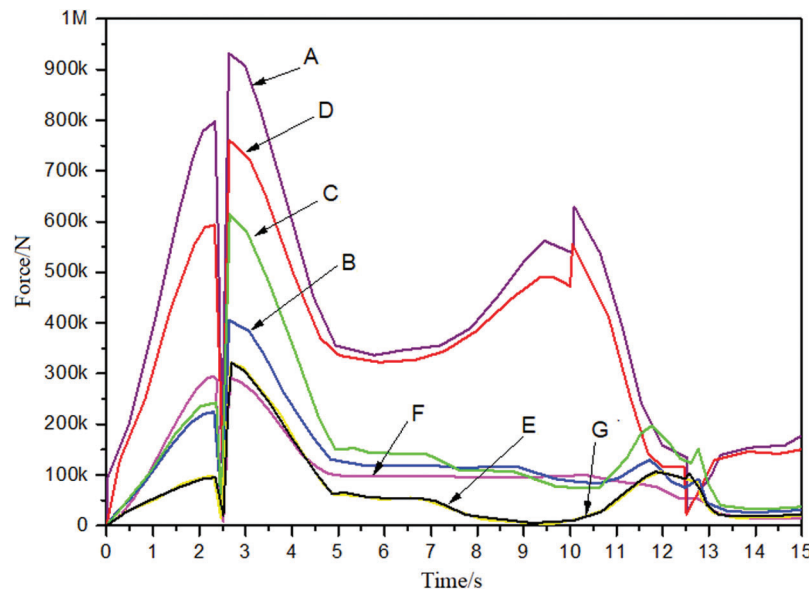


Figure 5: Force simulation curves of each hinge points of working device

6 Conclusions

- a) In the paper, we took the loader's working device as the subject. Firstly, through using Solidworks software, the 3D model of loader's working device is established. Secondly, simulation analysis was carried out by dynamic analysis software—ADAMS through importing the 3D model.
- b) The simulation analysis results showed that hinge points's force is basically consistent with the actual working conditions, which verifies the correctness of the simulation.
- c) The dynamic simulation with ADAMS software makes up for the shortcoming of traditional design which cannot be directly viewed and quickly analyzes the kinematic characteristics of the mechanism. It is an effective means to improve the efficiency of product design.
- d) The maximum load appears at the hinge of boom and front support during the operation of loader, where the maximum stress value is 930 kN.
- e) The dynamic analysis of the working device is carried out by using ADAMS software, which provides a theoretical reference for the design and improvement of the working device of the loader.

Funding Statement: Natural Science Foundation of Hunan Province (No. 2018JJ3478), Scientific Research Fund of Hunan Provincial Education Department (No. 15C1240) and Innovation platform open fund Project (No. 16K080) and Shao yang guiding science and technology plan project (2019ZD15).

Conflicts of Interest: The authors declare that they have no conflicts of interest to report regarding the present study.

References

1. Bo, S. J., Zhu, H., Ye, Q. H. (2013). Key technologies of rigid-flexible coupling system modeling and simulation. *Applied Mechanics and Materials*, 599–601, 652–655. DOI 10.4028/www.scientific.net/AMM.599-601.652.
2. Cao, B. T., Li, X. Y., Yang, Y. Q. (2014). Three dimensional modeling and finite element analysis of loader working device. *Coal Mine Machinery*, 35(5), 105–107.
3. Du, L., Peng, W. F., Huang, J. (2011). Simulation and research on mechanism-hydraulics system of working device of HT-25J wheel loader. *Electronic & Mechanical Engineering & Information Technology International Conference*, 5, 2497–2500.
4. Frank, R. (2015). Improved markets boost smaller wheel loaders. *Construction Equipment*, 8, 10–12.
5. Huang, C. Y., Su, S. H., Xu, K., Chen, C. (2016). Dynamics modeling and simulation of loader working device under unloading condition. *International Conference on Artificial Intelligence and Engineering Applications*. DOI 10.2991/aiea-16.2016.86
6. Zhang, G. J., Xiao, C. Y. (2018). Dynamic simulation analysis on loader's working device. *Australian Journal of Mechanical Engineering*, 16(sup1), 2–8.
7. Zheng, X. J., Mang, Q., Xie, Z. Y., Li, T. J. (2009). Kinematics and dynamics simulation analysis of wheel loader based-on ADAMS. *Machinery Design & Manufacture*, 41(10), 38–42.
8. Liu, W. H., Wang, L. Y., Liu, Y. (2013). Dynamic analysis of the working device of a wheel-type loader based on ADAMS. *Forestry Machinery & Woodworking Equipment*, 41(10), 38–42.
9. Li, F., Ma, C. L. (2003). Research on simulation and optimization for dynamical characteristics of hydraulic system based on SIMULINK. *Computer Simulation*, 20(5), 110–112.
10. Zhang, G. J., Xiao, C. Y., Tan, Q., Mo, Y. Y. (2014). Dynamic analysis and simulation of excavator working device based on virtual prototyping technology. *Journal of Central South University (Natural Science Edition)*, 45(6), 1827–1833.
11. Zhang, N. (2014). Virtual prototype and simulation analysis based on pro/E for work device of loader. *Mechanical Engineering & Automation*, 01, 32–33.
12. Zhang, X. H., Xie, H. S., Tang, Q. S. (2012). Co-simulation of mechanism-hydraulics working device of loader ZL-50 based on ADAMS. *Applied Mechanics & Materials*, 2049(233), 186–191.
13. Zou, N. W., Wei, Y. T., Zhou, D. S. (2015). Research on wheel loader duty cycle test and numerical expression. *Advanced Materials Research*, 3726, 154–159.
14. Li, L., Xu, D. P., Zhou, H. G., Hao, S. (2020). Analysis and control of movement characteristics of working machine of backhoe loader. *Machine Tool & Hydraulics*, 48(02), 163–170.
15. Wan, Y. P., Song, X. D., Yuan, Z. W., Yu, L. P. (2018). Statistical analysis on random load of working device of loader. *Journal of Hefei University of Technology (Natural Science)*, 41(10), 1302–1308.
16. Liu, G. H. (2018). Analysis of the thermal characteristics of the hydraulic system of the loader working device. *Petrochemical Industry Technology*, 25(09), 50.
17. Ji, X. (2017). *Study on elector-hydraulic control system characteristics of loader working device. (Master's Thesis)*. Liaoning Technical University, Liaoning, China.